RSC Advances

PAPER

Cite this: *RSC Adv.*, 2025, **15**, 16734

Coupling ozone-based AOPs with DLLME for simultaneous determination of trace free antimony and total antimony in surface water

Xiaofang Sun,* Chuanbin Zhang, Youwen Pan, Haiyang Mei, Jiawen Song and Mengfei Zhou

The traditional standard method for the determination of the heavy metal pollutant antimony (Sb) in water, 5-Br-PADAP spectrophotometry, involves the consumption of many kinds of chemical reagents and has low sensitivity. For highly toxic liquid and gas containing Sb(III), this paper presents a green determination method based on UV/O_3 synergistic oxidation-malachite green-dispersive liquid–liquid microextraction (DLLME)-spectrophotometry, which can achieve the enrichment of a trace amount of antimony in water and high-precision detection. Using the selective complexation and color development of protonated alkaline dye and the solubility difference of the complexes involved, an enrichment and determination method for trace Sb(V) in surface water was established for the first time. Based on the feature of the UV/O_3 system of rapid and complete oxidation of Sb(III), and the easy elimination of the disturbance of residual oxidant, the green determination method for trace total antimony (TSb) was constructed based on advanced oxidation processes (AOPs). To verify the validity of the proposed method, all the process parameters and environmental factors affecting the oxidation efficiency of Sb(III) and the enrichment performance of DLLME were investigated and optimized. The results showed that the proposed method exhibited good linearity (R^2 = 0.9943), a low method detection limit (MDL = 0.3208 μg L^{-1}), and high precision (1.63%) and accuracy (0.64%) in the range of 1–30 μg L^{-1}, under the optimized process conditions. By the difference method, the trace free antimony (Sb(III), Sb(V)) and total antimony (TSb) can be determined simultaneously.

Received 18th January 2025
Accepted 28th April 2025

DOI: 10.1039/d5ra00432b

rsc.li/rsc-advances

1. Introduction

Antimony (Sb), a heavy metal with a silvery lustre, exists in nature mainly in the form of the sulfide ore stibnite (Sb_2S_3).[1] 60% of antimony's downstream products are flame retardants, 25% are lead-acid batteries, and the remaining 15% include pharmaceuticals, military products, heat stabilizers,[2] photovoltaic glass, and solar cells.[3] Antimony plays a significant role in the manufacturing industry, and its demand has increased dramatically with societal development. Large quantities of antimony-containing substances are produced during the mining process, production of downstream products, and end-of-life disposal,[4,5] which cause damage to groundwater and surface water through soil runoff under the effect of rapid vertical infiltration.[6,7] Antimony and its compounds induce diseases by inhibiting the activity of enzymes related to ATP production in the body,[8] and even heart diseases such as myocarditis when ingested in large quantities over a short period of time. In the context of serious pollution, antimony contamination is being recognized as a global threat.[9] Antimony in nature is mainly found in four valence states: Sb(V), Sb(III), Sb(0), and Sb(-III).[10] Sb(III) and Sb(V) mainly exist in the surface water environment as well as in living organisms, with inorganic antimony(III) being about 10 times more toxic than inorganic antimony(V).[11,12] The United States requires that the antimony content of drinking water is less than 6 μg L^{-1}, the European Union regulates it at 5 μg L^{-1},[13] and China stipulates that it should not be higher than 5 μg L^{-1}. Antimony contamination in the surface water environment can directly affect public water safety.

There are numerous methods for detecting antimony in water, broadly classified into atomic fluorescence spectrometry (AFS),[14] atomic absorption spectrometry (AAS),[15] inductively coupled plasma mass spectrometry (ICP-MS),[16] electrochemical analysis,[17,18] spectrophotometry,[19] *etc.* Among them, methods such as AFS, AAS, and ICP-MS offer high detection accuracy and low detection limits, but the instruments used are expensive and require extensive sample pretreatment.[20,21] In electrochemical analysis, factors such as the influence of co-existing ions and the state of the electrode surface must be considered, and the uncertainty of the electrode state limits its potential for continuous detection.[22] However, the traditional photometric methods are complicated in operation, involve the addition of various chemical reagents, and pose potential

College of Chemical Engineering, Zhejiang University of Technology, Hangzhou, China. E-mail: zgdsxf@zjut.edu.cn

secondary contamination risks during the detection process. Many detection methods focus on the detection of Sb(III),[23–26] and emissions of waste liquid or gas containing a large amount of Sb(III) pose a greater toxicity risk and pressure on the environment. Antimony in natural waters often exists at trace or even ultra-trace concentrations, and in order to ensure the accuracy of detection results, it is necessary to develop a highly sensitive color development and enrichment method for water samples first, combined with the traditional spectrophotometric method (cheap price but low sensitivity) to achieve automatic online detection of antimony in water quality. The main enrichment methods for antimony-containing samples include adsorption, co-precipitation, and extraction, with the latter becoming the primary method due to the poor selectivity and numerous interfering factors associated with the first two methods. Extraction methods include single-drop microextraction (SDME), dispersive liquid–liquid microextraction (DLLME), and cloud point extraction (CPE). Oviedo *et al.*[27] detected Sb(III) using DLLME, while Biata *et al.*,[28] Hagarová *et al.*,[29] and Snigur *et al.*[30] detected Sb(III) using CPE, all achieving low detection limits but also encountering the issue of a large amount of Sb(III) existing in the discharged waste liquid. Therefore, it is of great practical significance to develop a new detection method for antimony in water that is safe, environmentally friendly, economical, efficient, and green.

In the present work, a novel and green detection method for trace heavy metal antimony in water was developed, based on UV/O_3 synergistic oxidation, malachite green–liquid–liquid microextraction, and spectrophotometry. In the proposed methodology, ultraviolet irradiation was used to activate O_3 for the synergistic oxidation of the highly toxic Sb(III) in water. Malachite green and liquid–liquid microextraction technology were then employed for the color development and enrichment of the oxidized Sb(V). Finally, spectrophotometry was used to accurately determine the Sb(V) concentration (total antimony). The approach also employs the difference method to determine the valence distribution of free antimony (Sb(III), Sb(V)) by measuring the Sb(V) concentration before and after the synergistic oxidation treatment. This approach is environmentally friendly, rapid, and of low cost, and requires mild reaction conditions, addressing many of the deficiencies in existing Sb(III) detection methods.

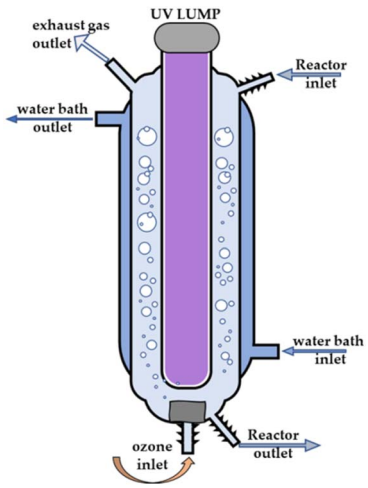

Fig. 1 Schematic diagram of a gas–liquid reactor.

2. Materials and methods

2.1 Instrumentation

The setup (self-made) for the UV/O_3 co-oxidation of Sb(III) in this experiment mainly consists of a jacketed gas–liquid reactor, a UV light source, an air-source ozone generator, a temperature-controlled water bath (thermostatic magnetic stirrer), and a circulating pump, as shown in the schematic diagram in Fig. 1.

The gas–liquid reactor, which is cylindrical and made of ordinary glass, has a 15 W UVC lamp at its center with a wavelength of 254 nm and a UVC intensity of 33–37 μW cm^{-2} at 1 m. This light intensity ensures that the solution within the gas–liquid reactor is fully irradiated, and the UVC lamp is protected by a quartz tube sheath. The temperature-controlled water bath is connected to a 24 VDC micro pump to circulate water from the bath into the jacket of the gas–liquid reactor to maintain the reaction temperature. Silicone tube is used to connect the reactor, the pump, and the temperature-controlled water bath. The cost of the experimental setup is shown in Table 1.

The main instruments used in this experiment for the enrichment and detection of antimony(V) by liquid–liquid microextraction methods were a centrifuge (ShangYi, Shanghai, China), an ultrasonic cleaner (KeXi, Beijing, China), and a UV-visible spectrophotometer (JINGHUA, Shanghai, China).

2.2 Reagents

All reagents used in the proposed method were analytical grade. Diphenylcarbazide solution at 20 mg L^{-1} was prepared using granular diphenylcarbazide (YONGHUA, Suzhou, China) in acetone (99.7%) (SINOPHARM, Beijing, China), followed by

Table 1 Installation cost

Number	Apparatus name	Model	Quantity	Unit price (CNY)
1	Gas–liquid reactor	Customization	1	500
2	UV light source	ZW15S8Y-D287	1	150
3	Air-source ozone generator	FL-10H-SCL	1	60
4	Temperature-controlled water bath	DF-101S	1	650
5	Circulating pump	KLC2	1	50

dilution with deionized water. Stock standard solutions at 1000 mg L^{-1} of Sb(v) or Sb(III) were prepared by dissolving potassium hexahydroxoantimonate (99.0%) (Aladdin, Shanghai, China) or potassium antimonyl tartrate (99.5%) (SINOPHARM, Beijing, China) in deionized water. Working solutions were prepared daily by diluting the previous solution with deionized water. NaOH solution (0.1 mol L^{-1}) was prepared by dissolving granular NaOH (MACKLIN, Hangzhou, China) in deionized water. Stock standard solution of malachite green (0.2%) was prepared by dissolving granular malachite green (MG) (BBI, Shanghai, China) in deionized water. The working solution was prepared daily by diluting the previous solution with deionized water. Stock standard solution at 1000 mg L^{-1} of Cr(VI) was directly purchased from Shanghai Aladdin Biochemical Technology Co., Ltd. The extractant used in this experiment is chlorobenzene (98%) (Titan, Shanghai, China), and the complexing agent is hydrochloric acid (99.99%) (Yonghua, Changshu, China). All other reagents used in this experiment were prepared using deionized water.

2.3 Principle of color development and enrichment for Sb(v)

In acidic solution, Sb^{5+} can quickly form the $[SbCl_6]^-$ complex anion with Cl^-. After the dissolution of malachite green in water, MG^+ can complex with $[SbCl_6]^-$ at a high concentration of hydrochloric acid to form an electrically neutral complex. This complex can be extracted with a small amount of chlorobenzene. Under ultrasonication, emulsification occurs, increasing the chance of contact between the small droplets of the organic phase and the antimony complex, and thus accelerating the rate of mass transfer. After short-time centrifugation to complete phase separation, the organic phase can be taken for detection (Fig. 2). The reaction process of the $MG[SbCl_6]$ complex is shown in eqn (1) and (2):

$$Sb^{5+} + 6Cl^- \rightarrow [SbCl_6]^- \quad (1)$$

$$[SbCl_6]^- + MG^+ \rightarrow MG[SbCl_6] \quad (2)$$

2.4 Methodological steps

(1) Turn on the circulating water pump and the constant temperature magnetic stirring device to stabilize the temperature inside the jacket of the gas–liquid reactor at 35 °C.

(2) Turn on the air-source ozone generator and air pump, and adjust the ozone flow rate to 0.3 L min^{-1}.

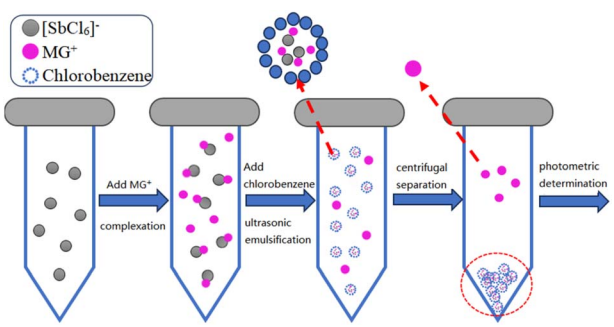

Fig. 2 Schematic diagram of the steps for liquid–liquid microextraction of Sb(v).

(3) Take 40 mL of the Sb(III) solution (working standard solutions or water samples), adjust the pH in range of 7 to 9 using hydrochloric acid and sodium hydroxide, and then inject it into the gas–liquid reactor.

(4) Turn on the UV lamp source and oxidate the water sample for 15 min.

(5) After stirring and allowing the solution to stand for 10 minutes, transfer 5 mL of the sample to a 10 mL centrifuge tube, add 3.33 mL of concentrated hydrochloric acid, dilute to 10 mL with deionised water, and shake well. At this point, the hydrochloric acid concentration in the 10 mL sample is approximately 4 mol L^{-1}.

(6) Continue to add 0.4 mL of the 0.02% malachite green working solution dropwise to the centrifuge tube and shake for 30 s.

(7) Quickly add 0.20 mL of chlorobenzene after shaking, and emulsify in an ultrasonic cleaner for 30 s.

(8) Place the centrifuge tube into a centrifuge and carry out centrifugal separation at 3500 rpm for 1 min, then carefully transfer the organic phase to a 700 μL microcuvette for photometric determination at an absorption wavelength of 628 nm, and calculate the total inorganic antimony in the water samples using the working curve of Sb(v).

2.5 Total antimony and Sb(III) determination

Prior to O_3 or UV/O_3 co-oxidation, the water sample to be tested is taken for Sb(v) determination by malachite green–liquid–liquid microextraction-spectrophotometry. The amounts of Sb(v) after O_3 oxidation and UV/O_3 co-oxidation of the water sample are determined as total inorganic antimony and total antimony, respectively, following the above procedure. Thus, Sb(III) and organic antimony can be determined from the difference between the total inorganic antimony and Sb(v).

3. Results and discussion

3.1 Factors affecting the synergistic oxidation of Sb(III) by UV/O_3

In this experiment, the hexavalent chromium oxidation method was used to indirectly detect the concentration of Sb(III) in solution, which is based on the principle that Cr(VI) can react with diphenylcarbazide to form a violet complex, and the concentration was determined by spectrophotometry ($\lambda = 540$ nm). While Cr(III) does not show color with diphenylcarbazide, the stoichiometric reaction of Cr(VI) being reduced to Cr(III) by Sb(III) was used to determine the concentration of Cr(VI) after the completion of the reaction to determine the amount of Sb(III) indirectly. The reaction equation is shown in eqn (3):

$$3Sb(III) + 2Cr(VI) \rightarrow 3Sb(V) + 2Cr(III) \quad (3)$$

Let the concentration of Sb(III) in the initial state be $[Sb_0(III)]$, and the concentration of Sb(III) at time t be $[Sb_t(III)]$, then the oxidation efficiency of Sb(III) is characterized by the conversion rate of Sb(III) in the solution at time t, CR, which is calculated as shown in eqn (4):

$$CR = \frac{[Sb_t(III)]}{Sb_0(III)} \quad (4)$$

Three parallel determinations were conducted for each experiment, and the average value of the three results was taken to explore the influencing factors.

3.1.1 Products of the synergistic oxidation of Sb(III) by UV/O_3. Before investigating the factors affecting the oxidation efficiency of Sb(III), the products of the oxidation of Sb(III) by the UV/O_3 system were first experimentally determined by fixing [Sb_0(III)] at 2 mg L^{-1} and taking samples every 2 min to determine the trends in the concentrations of Sb(III) and Sb(V) in the solution over oxidation time, and the results are shown in Fig. 3.

According to the experimental results, under the action of UV/O_3, with the prolongation of the reaction time, the decreasing trend in the concentration of Sb(III) and the increasing trend in Sb(V) are almost identical, proving that the synergistic oxidation of Sb(III) to Sb(V) by UV/O_3 is feasible under suitable conditions.

3.1.2 Effect of reaction temperature on oxidation efficiency. Temperature is an important process parameter during UV/O_3 oxidation and has a significant effect on the oxidation efficiency. In the UV/O_3 oxidation process, the reaction temperature needs to be properly controlled to achieve the desired oxidation efficiency. The results of Sb(V) concentration detected in the solution when oxidized at different reaction temperatures are shown in Fig. 4.

According to the experimental results, it can be concluded that the oxidation efficiency of Sb(III) increases and then decreases with the increase of reaction temperature, and the reaction temperature of 35 °C was selected, considering energy consumption and oxidation efficiency. The reason for the decrease in oxidation efficiency with the increase of reaction temperature may be that the survival time of free radicals becomes shorter with the increase of temperature, and at the same time, the solubility and concentration of ozone in the aqueous solution decrease, and the number of free radicals produced by the synergistic action of UV/O_3 becomes less.

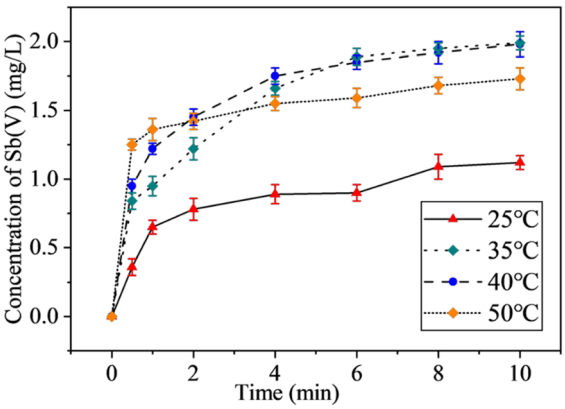

Fig. 4 Effect of reaction temperature on Sb(III) oxidation efficiency. Conditions: reaction temperature: 25 °C, 35 °C, 40 °C, and 50 °C; ozone flow: 0.4 L min^{-1}; oxidation time: 10 min; pH: 7; with all other conditions as per Section 2.4.

3.1.3 Effect of ozone flow on oxidation efficiency. Increasing the concentration of ozone in the aqueous solution is the key to increasing the UV/O_3 synergistic oxidation of antimony. Therefore, an appropriate ozone flow is needed in the gas–liquid reaction process. The concentration of Sb(V) was observed at different ozone flow rates, and the experimental results are shown in Fig. 5.

From the data in Fig. 5, it can be seen that the oxidation efficiency of Sb(III) increases with the increase of ozone flow rate and tends to stabilize when the flow rate is greater than 0.3 L min^{-1}. At this point, the concentration of Sb(V) tends to 2 mg L^{-1}, and the oxidation efficiency of Sb(III) in the water sample is close to 99%. For energy-saving and flooding considerations, the optimum ozone flow rate was selected to be 0.3 L min^{-1}.

3.1.4 Effect of pH on oxidation efficiency. The pH has a strong influence not only on the speciation of antimony in an ambient medium[31] but also on the speciation of ozone in water.

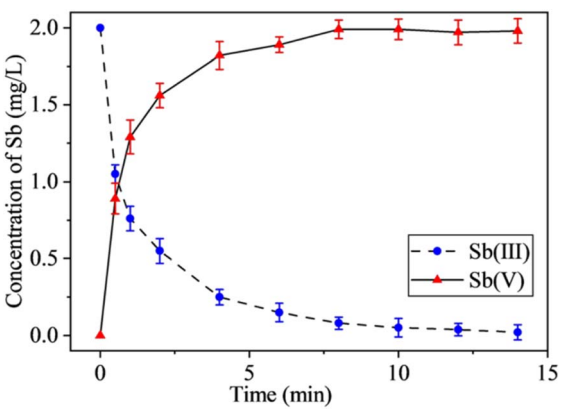

Fig. 3 Concentration of Sb(V) and Sb(III) in solution. Conditions: reaction temperature: 40 °C; ozone flow: 0.4 L min^{-1}; pH: 7; with all other conditions as per Section 2.4.

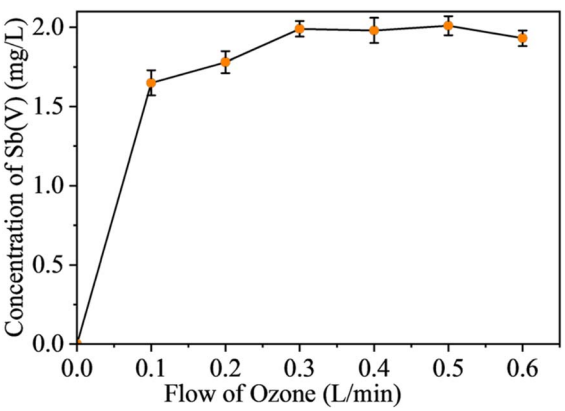

Fig. 5 Effect of ozone flow on Sb(III) oxidation efficiency. Conditions: reaction temperature: 35 °C; ozone flow: 0.1 L min^{-1}, 0.2 L min^{-1}, 0.3 L min^{-1}, 0.4 L min^{-1}, 0.5 L min^{-1}, and 0.6 L min^{-1}; oxidation time: 10 min; pH: 7; with all other conditions as per Section 2.4.

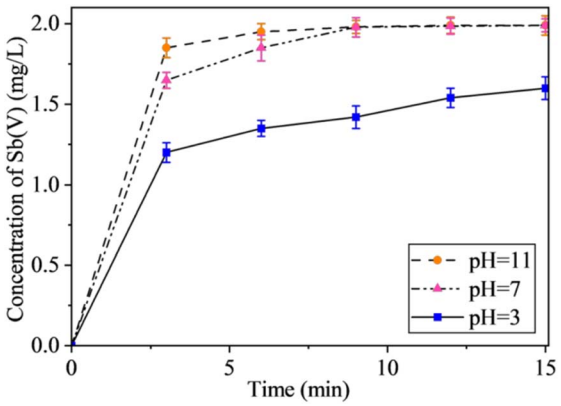

Fig. 6 Effect of different pH values on Sb(III) oxidation efficiency. Conditions: reaction temperature: 35 °C; ozone flow: 0.3 L min^{-1}; pH: 3, 7, and 11; with all other conditions as per Section 2.4.

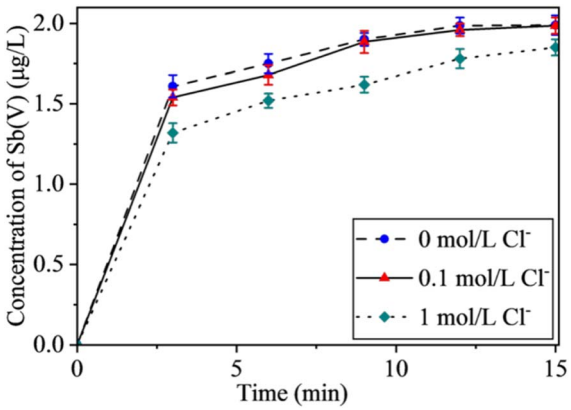

Fig. 7 Effect of Cl^- concentration on Sb(III) oxidation efficiency. Conditions: Cl^- concentration: 0.1 mol L^{-1} and 1 mol L^{-1}; pH: 5–6, with all other conditions as per Section 2.4.

The oxidation time was fixed at 15 min, and the concentration of Sb(V) in the solution was detected by taking samples at 3-minute intervals. The oxidation efficiency of UV/O_3 for Sb(III) was observed at different pH values, and the experimental results are shown in Fig. 6.

From Fig. 6, it can be seen that the conversion rate of Sb(III) by UV/O_3 co-oxidation increased with increasing pH, and the conversion rate of Sb(III) reached close to 98% at pH = 11 and an oxidation time of 6 min. Besides, the conversion rate of Sb(III) was close to 100% at pH = 7 and an oxidation time of 9 min. At pH = 3, the oxidation efficiency of Sb(III) was found to be affected, and only 80% of Sb(III) was oxidized after 15 min. The reason may be that the oxidation of Sb(III) is dominated by O_3 in acidic environments, and the large amount of H^+ in the solution inhibited the conversion of $^{\cdot}OH$, which led to the decrease of the oxidation efficiency. Simultaneously, the large amount of Cl^- added during pH adjustment consumed most of the $^{\cdot}OH$, which also led to the decrease of the oxidation efficiency. It can be seen that the oxidation efficiency of Sb(III) is different at different pH levels. In the range of pH = 7–11, Sb(III) can be completely oxidized within 10 min.

3.1.5 Effect of inorganic ions on oxidation efficiency. In natural water bodies, water samples usually contain complex inorganic anions such as Cl^-, NO_3^-, CO_3^{2-} and HCO_3^-, which will consume •OH to varying degrees in the UV/O_3 co-oxidation system, thus affecting the oxidation efficiency of Sb(III). In order to investigate and verify the applicability of the UV/O_3 co-oxidation method, three common inorganic anions, Cl^-, NO_3^- and HCO_3^-, in surface water, drinking water, and wastewater were selected under different pH environments to study their effects on the oxidation efficiency of Sb(III), and the experimental results are shown in Fig. 7–9.

According to Fig. 7, when the concentration of Cl^- is 0.1 mol L^{-1} in water, there is almost no interference with the oxidation of antimony. When it reaches 1 mol L^{-1}, it has a significant impact on the oxidation efficiency of Sb(III). The main reason is that under weakly acidic conditions, $^{\cdot}OH$ contributes more to the oxidation of Sb(III), but the high concentration of Cl^- consumes a large amount of $^{\cdot}OH$ in water, resulting in the reduction of the oxidation efficiency of Sb(III).

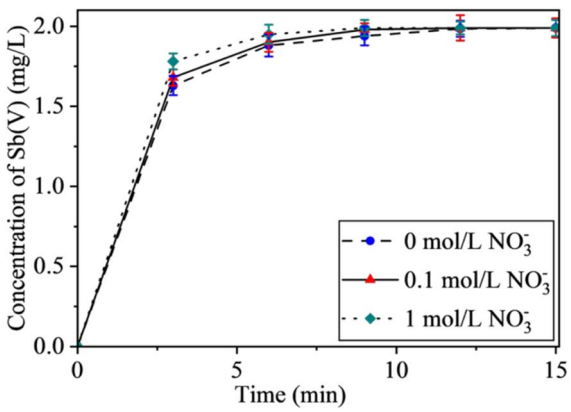

Fig. 8 Effect of NO^{3-} concentration on Sb(III) oxidation efficiency. Conditions: NO_3^- concentration: 0.1 mol L^{-1} and 1 mol L^{-1}; pH: 7; with all other steps as per Section 2.4.

According to Fig. 8, it can be seen that in a neutral environment, a low concentration of NO_3^- has a slight effect on the oxidation efficiency of antimony. When the concentration of NO_3^- in water is 1 mol L^{-1} and the oxidation time is 6 min, the conversion rate of Sb(III) reaches 97.5%, which is higher than the efficiency without NO_3^-. This indicates that NO_3^- promotes the oxidation of Sb(III) to a certain extent, but the contribution of $^{\cdot}NO_2$ to the oxidation of Sb(III) in this process is still unclear.

According to Fig. 9, when the concentration of CO_3^{2-} in the water sample is 0.1 mol L^{-1}, there is obvious interference of Sb(III), but Sb(III) can still be completely oxidized within 15 min. When the concentration of CO_3^{2-} is 1 mol L^{-1}, the ability of the UV/O_3 system to oxidize Sb(III) is slightly decreased compared with that at 0.1 mol L^{-1}, and Sb(III) can be completely oxidized in 15 min. In general, the concentration of CO_3^{2-} has little effect on the oxidation.

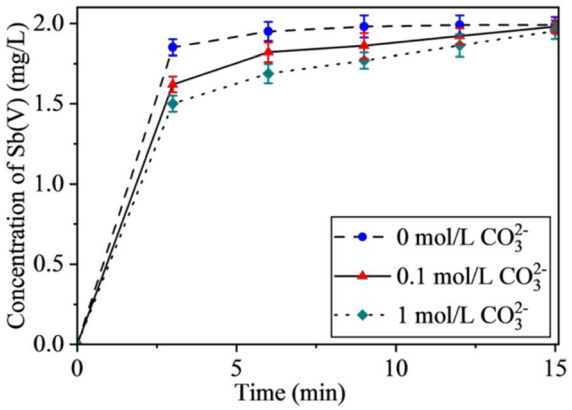

Fig. 9 Effect of CO_3^{2-} concentration on Sb(III) oxidation efficiency. Conditions: CO_3^{2-} concentration: 0.1 mol L^{-1} and 1 mol L^{-1}; pH: 11; with all other steps as per Section 2.4.

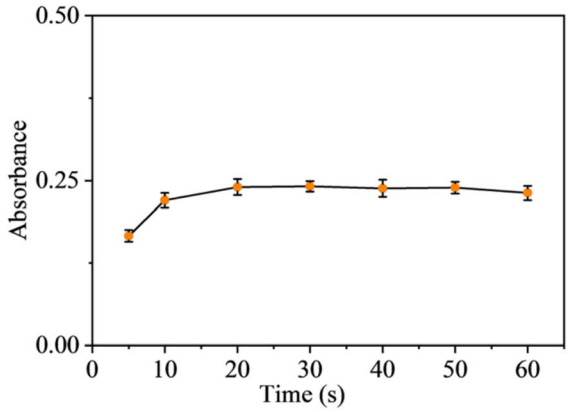

Fig. 11 Effect of sonication time on LLME. Conditions: hydrochloric acid concentration in the 10 mL sample: 2.4 mol L^{-1}; with all other steps as per Section 2.4.

3.2 Factors affecting the liquid–liquid microextraction

3.2.1 Effect of malachite green concentration on LLME. The absorbance changes in the organic phase at malachite green concentrations of 0.005%, 0.01%, 0.02%, 0.04%, 0.06%, 0.08%, and 0.10% are depicted in Fig. 10.

According to the data in the graph, it can be observed that the absorbance of the organic phase increases progressively with increasing malachite green concentration, and when the concentration is more than 0.02%, the absorbance of the organic phase fluctuates slightly, but the change is not significant. Therefore, a malachite green concentration of 0.02% was chosen for subsequent optimization experiments.

3.2.2 Effect of sonication time on LLME. The absorbance changes in the organic phase at sonication times of 5 s, 10 s, 20 s, 30 s, 40 s, 50 s, and 60 s are shown in Fig. 11.

From Fig. 11, it is observed that the absorbance of the organic phase begins to increase with increasing sonication time, when the ultrasonic emulsification treatment time was greater than 20 s, the organic phase absorbance did not change much, and when the treatment time was greater than 50 s, there was a small decrease in absorbance. This may be due to the fact that some of the MG[$SbCl_6$] complexes were destroyed by the ultrasonic energy and de-complexed, and the MG^+ returned to the aqueous phase, resulting in a decrease in the amount of MG[$SbCl_6$] extracted into the organic phase.

3.2.3 Effect of hydrochloric acid concentration on LLME. The absorbance changes in the organic phase upon adding 2.08 mL, 2.50 mL, 2.91 mL, 3.33 mL, 3.75 mL, 4.17 mL, and 5.00 mL of hydrochloric acid are shown in Fig. 12.

The results showed that the absorbance of the organic phase gradually increased with the increase of hydrochloric acid concentration, and began to decrease when the hydrochloric acid concentration was greater than 4 mol L^{-1} (3.33 mL). The optimum concentration of hydrochloric acid was chosen as 4 mol L^{-1}.

Through the investigation of single factor experiments, the optimized extraction conditions of the malachite green-liquid-liquid microextraction-spectrophotometry for the determination of antimony are as follows: 5.0 mL water sample; 3.33 mL of concentrated hydrochloric acid; 400 μL malachite green with a concentration of 0.02%; 0.2 mL chlorobenzene; sonication time of 20 s.

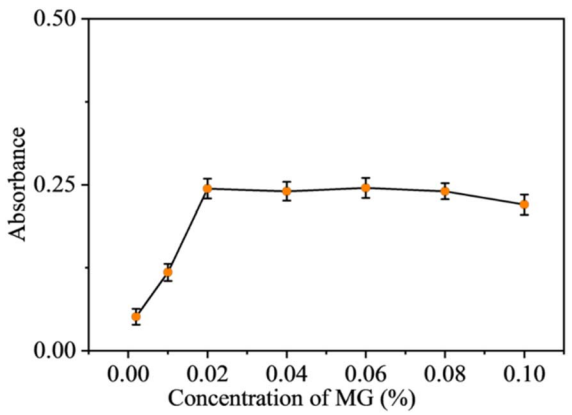

Fig. 10 Effect of malachite green concentration on LLME. Conditions: hydrochloric acid concentration in the 10 mL sample: 2.4 mol L^{-1}; with all other steps as per Section 2.4.

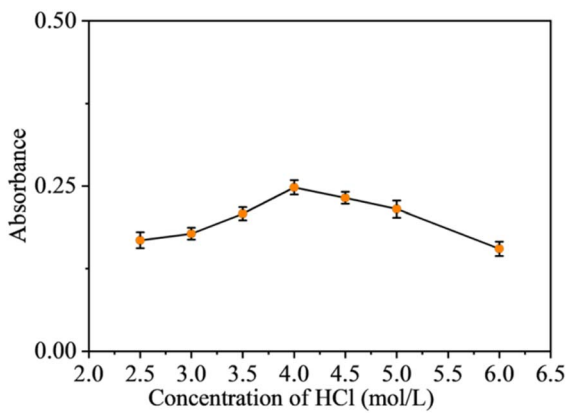

Fig. 12 Effect of HCl concentration on LLME. Conditions: malachite green concentration: 0.02%; sonication time: 30 s; with all other steps as per Section 2.4.

3.3 Analytical performance

3.3.1 Working curve. The standard solution was prepared from Sb(III) stock standard solution at concentrations of 1–30 μg L^{-1}, and then co-oxidized by UV/O_3 under the above optimal conditions for determination. The absorbance of the blank was measured after treatment using deionised water instead of the sample, and the results are shown in Fig. 13. The equation of the working curve for Sb(V) after oxidation by UV/O_3 was obtained in the range of 1–30 μg L^{-1}: $y = 0.0091x + 0.0155$ ($R^2 = 0.9943$), where x represents the concentration of Sb(V), and y is the net absorbance measured after oxidation by UV/O_3.

3.3.2 Method detection limit. The absorbance of the sample (A_s) measured by the optimized UV/O_3 synergistic oxidation-malachite green-liquid-liquid microextraction-spectrophotometry (AOPs-MG-LLME-Vis), and the blank absorbance (A_b) were measured by repeating the above procedure with deionised water in place of the sample, and the measurement was carried out eight times ($n = 8$, $t = 2.998$) in parallel. The experimental results are shown in Table 2. The method detection limit (MDL) for the determination of trace Sb(V) was calculated to be approximately 0.3208 μg L^{-1}.

3.3.3 Precision and accuracy. Sb(III) solutions were further prepared at concentrations of 6 μg L^{-1} and 24 μg L^{-1}. The net absorbance of the samples was determined, and the concentrations were calculated according to the optimised AOPs-MG-LLME-Vis method. The calculated precision and accuracy results are shown in Table 3. The precision of the proposed method for the determination of trace Sb(V) was calculated to be 1.63%, and the accuracy was 0.64%. Lima *et al.*,[32] Correia *et al.*,[33] Jakavula *et al.*,[16] Moradi *et al.*,[24] and Biata *et al.*[28] employed methods such as AFS, AAS, and ICP-OES for antimony detection in water, achieving precision levels ranging from 2.4% to 4.7% and accuracy values all exceeding 0.7%.

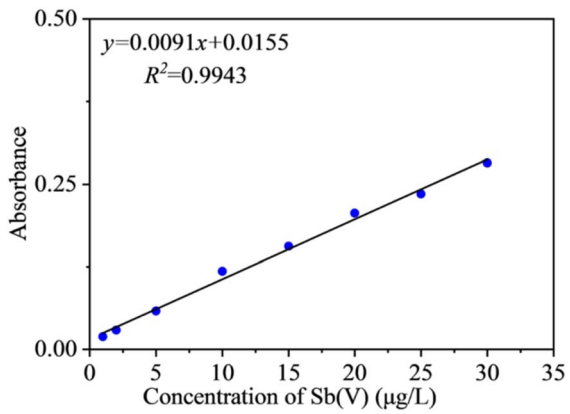

Fig. 13 Sb(V) working curve. Conditions: with all other steps as per Section 2.4.

Table 2 Blank experiment results table (AOPs-MG-LLME-Vis)

Number	Blank concentration value (μg L^{-1})	Average concentration value (μg L^{-1})	Standard deviation (S)
1	−0.1429		
2	−0.1099		
3	0.0110		
4	0.0770	−0.1181	0.1070
5	−0.1868		
6	−0.2198		
7	−0.1758		
8	−0.1978		

Table 3 AOPs- LLME method accuracy test

Number	Standard sample concentration 6 μg L^{-1}	Standard sample concentration 24 μg L^{-1}
1	6.1233	24.1205
2	6.0195	24.2201
3	5.8995	23.7895
4	6.1025	24.0018
5	5.9514	23.8541
6	6.1358	23.5569
Mean value	6.0387	23.9238
Relative standard deviation (%)	1.63	1.01
Relative error (%)	0.64	−0.32
Precision (%)	1.63	
Accuracy (%)	0.64	

Through performance evaluation, our method demonstrates superior precision and accuracy compared to most existing techniques for trace antimony detection in water. However, its detection limit remains higher than those of widely used methods like HG-AFS, HG-AAS, and ICP-OES. Future efforts should focus on optimizing enrichment strategies to further reduce the detection limit and enhance sensitivity.

4. Conclusions

In this paper, a novel and green method based on O_3 or UV/O_3 synergistic oxidation technology and malachite green-dispersive liquid–liquid microextraction-spectrophotometry is employed for the enrichment and high-precision determination of trace antimony (TSb, Sb(V) and Sb(III)) in water. Through single-factor experiments, all the process parameters and environmental factors affecting the oxidation efficiency of Sb(III) and the enrichment performance of dispersive liquid–liquid microextraction (DLLME) were analyzed, and all the process conditions of the proposed method were optimized, resulting in a detection process that is green, fast, and low-cost, and has mild reaction conditions.

The determination of trace antimony(V) using liquid–liquid microextraction technology is a novel enrichment detection method, which can significantly reduce the use of extractants, minimize secondary pollution, and render the final waste liquid virtually free of antimony(III) through the oxidation treatment of water samples, making it more environmentally friendly. This method employs spectrophotometric detection and is therefore not suitable for determining the antimony content in naturally colored water samples due to potential interference from

intrinsic chromophores. The proposed method, requiring only a trace amount of extractant and based on the determination of Sb(v), is expected to become a green and promising alternative to mainstream Sb(III) detection methods.

Data availability

The datasets generated or analyzed during the current study are not publicly available due to restrictions, for example, privacy or ethical but are available from the corresponding author on reasonable request.

Author contributions

Xiaofang Sun: conceptualization; data curation; formal analysis; funding acquisition; investigation; methodology; project administration; resources; supervision; validation; writing; reviewing and editing. Chuanbin Zhang: conceptualization; data curation; formal analysis; investigation; designing of the methodology; validation; writing; editing. Youwen Pan: investigation; methodology; writing; editing. Haiyang Mei: investigation; methodology; Jiawen Song: investigation; methodology; Mengfei Zhou: data curation; investigation; project administration; resources.

Conflicts of interest

The authors declare that they have no financial interests or personal relationships that could have influenced the work reported in this document.

Acknowledgements

This work was supported by Zhejiang Provincial Natural Science Foundation of China under grant no. LTGS24B070007.

References

1 Q. Guo, B. Planer-Friedrich, L. Luo, M. Liu, G. Wu, Y. Li and Q. Zhao, *Environ. Pollut.*, 2020, **266**, 0269–7491.
2 M. L. C. M. Henckens, P. P. J. Driessen and E. Worrel, *Resour., Conserv. Recycl.*, 2016, **108**, 54–62.
3 J. Wang, K. Li, J. Tang and C. Chen, *Sol. RRL*, 2023, **7**, 2300436.
4 A. Turner and M. Filella, *Sci. Total Environ.*, 2017, **584**, 982–989.
5 A. Parviainen, E. M. Papaslioti, M. Casares-Porcel and C. J. Garrido, *Environ. Pollut.*, 2020, **263**, 114482.
6 M. Filella, N. Belzile and Y. W. Chen, *Earth-Sci. Rev.*, 2002, **57**, 125–176.
7 B. Wen, J. Zhou, P. Tang, X. Jia, W. Zhou and J. Huang, *J. Hazard. Mater.*, 2023, **446**, 130622.
8 M. A. Tirmenstein, P. I. Mathias, J. E. Snawder, H. E. Wey and M. Wey, *Toxicology*, 1997, **119**, 203–211.
9 Y. Tao, H. Su, H. Li, Y. Zhu, D. Shi, F. Wu and F. Sun, *J. Cleaner Prod.*, 2021, **318**, 128514.
10 Y. Qin, X. Tang, X. Zhong, Y. Zeng, W. Zhang, L. Xin and L. Zhang, *Int. J. Biol. Macromol.*, 2024, **257**, 128615.
11 X. Liu, J. Zhou, W. Zhou, Y. Feng, Y. Z. Finfrock, Y. Liu, P. Liu and C. Shu, *J. Environ. Chem. Eng.*, 2021, **9**, 106741.
12 F. Liendo, A. P. de la Vega, M. J. Aguirre, F. Godoy and R. Segura, *Food Chem.*, 2022, **367**, 130676.
13 G. Ungureanu, S. Santos, R. Boaventura and C. Botelho, *J. Environ. Manage.*, 2015, **151**, 326–342.
14 P. Cava-Montesinos, M. L. Cervera, A. Pastor and M. de la Guardia, *Talanta*, 2003, **60**, 787–799.
15 I. Koch, L. Wang, J. Feldmann, P. l Andrewes, K. J. Reimer and W. R. Cullen, *Int. J. Environ. Anal. Chem.*, 2000, **77**, 111–131.
16 S. Jakavula, N. R. Biata, K. M. Dimpe, V. E. Pakade and P. N. Nomngongo, *Polymers*, 2022, **14**, 21.
17 K. Zarei, M. Atabati and M. Karami, *J. Hazard. Mater.*, 2010, **179**, 840–844.
18 H. V. Sezgin, Y. Dilgin and H. İ. Gökçel, *Talanta*, 2017, **164**, 677–683.
19 M. Gallignani, F. Ovalles, M. del Rosario Brunetto, M. Burguera and J. L. Burguera, *Talanta*, 2005, **68**, 365–373.
20 L. A. Portugal, L. Ferrer, A. M. Serra, D. G. da Silva, S. L. C. Ferreira and V. Cerdà, *J. Anal. At. Spectrom.*, 2015, **30**, 1133–1141.
21 L. L. G. de Oliveira, G. O. Ferreira, F. A. C. Suquila, F. G. de Almeida, L. A. Bertoldo, M. G. Segatelli, E. S. Ribeiro and C. R. T. Tarley, *Food Chem.*, 2019, **294**, 405–413.
22 A. V. Kolliopoulos, J. P. Metters and C. E. Banks, *Anal. Methods*, 2013, **5**, 3490–3496.
23 S. Rath, W. F. Jardim and J. G. Dórea, *J. Anal. Chem.*, 1997, **358**, 548–550.
24 M. Moradi, S. Zarabi and R. Heydari, *Chem. Pap.*, 2021, **75**, 6499–6508.
25 O. Yağmuroğlu, *Environ. Monit. Assess.*, 2022, **195**, 191.
26 H. B. Zengin and R. Gürkan, *J. Food Compos. Anal.*, 2023, **115**, 104931.
27 M. N. Oviedo, E. F Fiorentini, A. A Lemos and R. G. Wuilloud, *Anal. Methods*, 2021, **13**, 1033–1042.
28 N. R. Biata, G. P. Mashile, J. Ramontja, N. Mketo and P. N. Nomngongo, *J. Food Compos. Anal.*, 2019, **76**, 14–21.
29 I. Hagarová and L. Nemček, *Sustain. Agric. Res.*, 2021, **52**, 49–77.
30 D. Snigur, E. A. Azooz, O. Zhukovetska, O. Guzenko and W. Mortada, *Trends Anal. Chem.*, 2023, **164**, 117113.
31 G. Li, Y. Xin, X. Lü, Q. Tian, K. Yan and L. Ye, *Trans. Nonferrous Met. Soc.*, 2020, **30**, 3379–3389.
32 E. A. Lima, F. A. S. Cunha, M. M. S. Junior, W. S. Lyra, J. C. C. Santos, S. L. C. Ferreira, M. C. U Araujo and L. F Almeida, *Talanta*, 2020, **207**, 119834.
33 F. O. Correia, T. S. Almeida, R. L. Garcia, A. F. S. Queiroz, P. Smichowski, G. O. D. Rocha and R. G. O. Araujo, *Environ. Sci. Pollut.*, 2019, **26**, 21416–21424.